Journal of Materials Chemistry A

RSC Publishing

PAPER

View Article Online
View Journal | View Issue

In situ synthesis of lithium sulfide–carbon composites as cathode materials for rechargeable lithium batteries†

Cite this: *J. Mater. Chem. A*, 2013, **1**, 1433

Zichao Yang,[a] Juchen Guo,[a] Shyamal K. Das,[a] Yingchao Yu,[b] Zhehao Zhou,[a] Héctor D. Abruña[b] and Lynden A. Archer*[a]

Lithium–sulfur batteries are among the most promising candidates for next-generation rechargeable lithium batteries in view of recent progress on sulfur–carbon composite cathodes. However, further progress on such batteries is hampered by their concomitant need for a metallic lithium anode, which introduces new challenges associated with uneven electrodeposition and lithium dendrite formation. Here we report a method of creating lithium sulfide–carbon composites as cathode materials, which can be paired with high-capacity anodes other than metallic lithium. Lithium sulfide is dispersed in a porous carbon matrix, which serves to improve its electrical conductivity and provides a framework for sequestration of sulfur and lithium polysulfides. The *in situ* synthesis approach allows facile, scalable synthesis of lithium sulfide–carbon composite materials that exhibit improved electrochemical properties. We also investigate the effect of lithium polysulfides dissolved in the electrolyte on the stability and cycling behavior of Li_2S–carbon composite cathodes.

Received 21st October 2012
Accepted 19th November 2012

DOI: 10.1039/c2ta00779g

www.rsc.org/MaterialsA

Introduction

Rising world energy demand and widespread interest in lowering mankind's carbon footprint is driving efforts worldwide to reduce reliance on fossil fuels for electrical power generation and transportation. The inherent intermittency of energy supplies from most renewable sources and the need for portability have elevated energy storage technologies in general, and rechargeable/secondary batteries in particular, as important enabling technologies. Lithium-ion batteries are among the most promising and fastest growing technologies in the energy storage sector.[1] Nagging challenges associated with safety, cost, storage capacity, and reliability have limited their adoption as the electrochemical storage technology of choice.

Elemental sulfur (S_8) has a theoretical specific storage capacity of 1675 mA h g^{-1}, the highest among solid cathode materials of interest for rechargeable lithium batteries. A lithium battery with sulfur as cathode and metallic lithium as anode has a theoretical specific energy of 2600 W h kg^{-1}. Even taking into account the fact that practical specific energy of lithium batteries is around 1/3 of the theoretical value, a Li–S battery offers a specific energy of ~800 W h kg^{-1}, a factor of 4 or more improvement over the practical specific energy available from any existing rechargeable battery technology. The success of a lithium–sulfur cell requires solutions to at least three technical challenges.[2–8] First, the low conductivity of sulfur and its reduction compounds, sulfides, limits material utilization in the battery cathode and restricts operation to low rates/currents. Second, the cell uses a lithium metal electrode, which may form dendrite deposits during repeated cycles of charge and discharge, with potentially disastrous consequences if a volatile electrolyte and/or flammable electrolyte ingredients are used in the battery. Finally, elemental sulfur forms a variety of salt allotropes of the Li_2S_n type termed lithium polysulfides, which exhibit varying levels of solubility in aprotic, liquid electrolytes.

Significant recent efforts have focused on developing a solution for the last of these problems.[7–11] The *lower order* lithium polysulfides with $n < 3$ display little to no solubility in the electrolytes and are hence retained in the cathode after the battery discharges, *higher order* polysulfides ($n > 4$) readily dissolve in the electrolyte, eroding the cathode during each discharge, causing the battery storage capacity to rapidly degrade/fade.[2] Higher order lithium polysulfides (Li_2S_n with $n > 4$) formed at the cathode may also diffuse through the electrolyte to the anode and react with the metallic lithium to form lower order polysulfides, which can diffuse back to the cathode to reform higher order Li_2S_n. This loop known as the shuttling reaction can continue indefinitely in a lithium–sulfur cell and lowers the coulombic efficiency. Approaches based on addition of electrolyte additives to tailor Li_2S_n solubility,[3,4] synthesis of polymer–sulfur composites,[5,6] and physical sequestration of the sulfur in porous carbons to form carbon–sulfur composites[7–13] have proven by far to be the

[a]*School of Chemical and Biomolecular Engineering, Cornell University, Ithaca, NY 14853, USA. E-mail: laa25@cornell.edu*

[b]*Department of Chemistry and Chemical Biology, Cornell University, Ithaca, NY 14853, USA*

† Electronic supplementary information (ESI) available. See DOI: 10.1039/c2ta00779g

most successful strategies for controlling the shuttle reaction and for improving battery performance over many charge–discharge cycles. If the carbon framework is electrically conductive, the last of the above methods also potentially provides a remedy for the low conductivity of sulfur and sulfides, and lithium–sulfur cells using this approach are currently considered the most promising candidates for a commercial lithium–sulfur battery that achieves its potential.

A lithiated sulfur cathode that takes advantage of these advances has been the subject of a few recent studies.[17,18] Unlike elemental sulfur, such a cathode can be used in conjunction with high-capacity delithiated anodes, such as Si or Sn, to form high-energy lithium ion batteries that are not prone to failure by short circuiting produced by lithium dendrite proliferation. Li_2S has a theoretical capacity of 1166 mA h g^{-1}, which when paired with a Si anode yields a Li_2S–Si lithium ion cell with a high theoretical specific energy of 1550 W h kg^{-1}. Prototype batteries based on such Li_2S/Sn[14] and Li_2S/Si[15] cells have been reported, but significant additional efforts are needed to achieve rechargeable batteries that live-up to the potential of the active materials in both the cathode and anode. Recent effort has been reported on the effective utilization of Li_2S which relies on charging the cell to 4 V in the first cycle to completely delithiate Li_2S.[16]

In this work, we report a new approach for synthesizing lithium sulfide–carbon (Li_2S@C) nanocomposites and evaluate the materials as cathodes for lithium-ion batteries. Additionally, we investigate the effect of dissolved Li_2S_n in the electrolyte on the electrochemical properties of Li_2S@C cathodes.

Experimental

Materials synthesis

Chemical reagents were purchased from Sigma-Aldrich unless otherwise stated and used without purification. 1.8 g of resorcinol, 6 g of lithium sulfate and 7 mg of sodium carbonate were dissolved in 70 ml of water, to which 2.7 ml of 30% formaldehyde solution was added. The solution was loaded into a Teflon-lined stainless steel autoclave and heated at 180 °C for 12 h. The resulting gel was centrifuged and the precipitate was collected and freeze-dried overnight. The solid obtained was heated in a tube furnace under argon atmosphere at 900 °C for 2 h using a ramp rate of 5 °C min^{-1} to obtain the final product. For lithium polysulfide preparation, 920 mg Li_2S, 3.2 g sulfur and 0.5 g lithium powder (from FMC Lithium) were added to 5 ml tetraglyme (tetraethylene glycol dimethyl ether) and stirred for 24 h. The mixture was filtered to obtain a dark reddish liquid. For more dilute solutions of lithium polysulfide, this liquid is diluted with either pure tetraglyme (for spectroscopy and elemental analysis) or solutions of LiTFSI in tetraglyme (for conductivity and electrochemical measurements) to obtain the desired concentrations.

Characterization

The crystal structures of the particles were characterized using a Scintag Theta-theta PAD-X X-Ray Diffractometer (Cu K_α, λ = 1.5406 Å). Their morphologies were studied using a FEI Tecnai G2 T12 Spirit Transmission Electron Microscope (120 kV) and elemental mapping (EDX and EELS) was performed using a FEI Tecnai F20 Transmission Electron Microscope (200 kV). Thermogravimetric analysis was performed using a TA Instruments Q5000 IR Thermogravimetric Analyzer. Raman spectra were taken using a Renishaw InVia Confocal Raman Microscope. UV-visible spectra were taken using a Molecular Devices SpectraMax M2e spectrophotometer. Nitrogen adsorption analysis for porous materials was performed using a Micromeritics ASAP 2020 Accelerated Surface Area and Porosimetry System. Elemental analysis (atomic emission spectroscopy) was performed using a Thermo Scientific iCAP 6500 ICP spectrometer. Ionic conductivities were measured using a Novocontrol N40 broadband dielectric spectrometer.

Electrochemical characterization

Electrochemical characterization of the Li_2S@C nanocomposites as cathode materials in rechargeable lithium batteries was performed at room temperature in 2032 coin-type cells. The working electrode consisted of 80 wt% of the active material, 10 wt% of carbon black (Super-P Li from TIMCAL) as a conductivity aid, and 10 wt% of polymer binder (PVDF, polyvinylidene fluoride, Aldrich). Aluminum foil (0.004 in thick, Alfa Aesar) was used as the current collector. Electrode casting was performed in the glove box as Li_2S is sensitive to moisture. Lithium foil (0.03 in thick, Alfa Aesar) was used as the counter and reference electrode. A 1 M solution of LiTFSI in tetraglyme, or solutions containing lithium polysulfides described above, were used as the electrolyte. Celgard 2500 polypropylene membranes were used as the separator. Assembly of cell was performed in a glove box with moisture and oxygen concentrations below 0.1 ppm. The room-temperature electrode capacities were measured using Neware CT-3008 battery testers and cyclic voltammetry was performed with a CH Instruments CHI600D potentiostat. Electrochemical impedance spectroscopy was performed with a Solartron Model 1252 Electrochemistry Workstation with a frequency response analyzer.

Results and discussion

The lithium sulfide–carbon (Li_2S@C) composite was synthesized using an *in situ* approach[19,20] designed to produce a uniform distribution of Li_2S in a carbon host. The method is illustrated in Fig. 1. Li_2S is formed through the reaction $Li_2SO_4 + 2C \rightarrow Li_2S + 2CO_2$. The reduction of sulfates to sulfides by carbon has long been utilized in the Leblanc process. Bulk lithium sulfide has been used as the precursor for Li_2S@C composites in a few reports.[14,17] The price of Li_2S is an order of magnitude higher than common lithium precursors such as lithium carbonate, suggesting that this choice is perhaps not the best for a battery cathode material. Here we focus instead on a lithium sulfate precursor, which seems a more promising candidate for eventual large-scale economical synthesis of Li_2S@C composite cathodes.

The carbon framework is formed by pyrolysis of a resorcinol–formaldehyde aerogel (RF gel). Resorcinol and formaldehyde

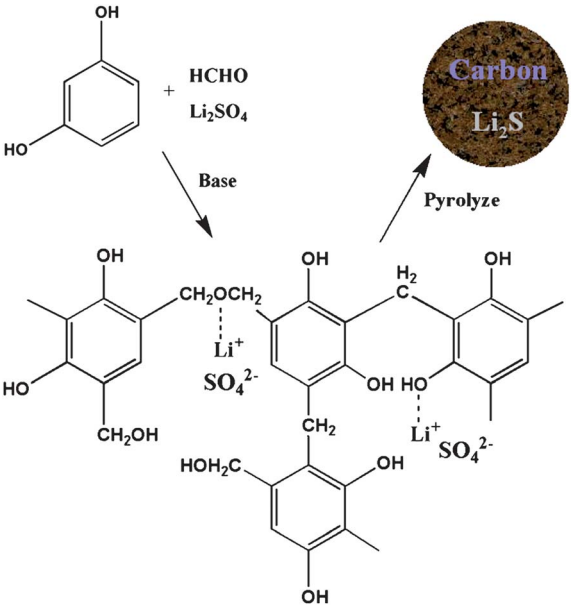

Fig. 1 *In situ* synthesis scheme for a Li_2S@C composite.

are known to undergo condensation polymerization under basic or acidic conditions to form a cross-linked gel known as the RF gel.[18] RF gel-based carbon materials have been promising candidates for various applications such as adsorbents, catalysts and battery/supercapacitor electrodes because of their high porosities and surface areas, high electrical conductivities and controllable pore structures.[19] We hypothesize that the large numbers of oxygen atoms present in the RF gel may form coordination-like linkages with lithium ions in Li_2SO_4, facilitating its uniform dispersion in the host material. Fig. 2 shows the X-ray diffraction pattern of the Li_2S composite synthesized using the *in situ* approach, and the pattern is unambiguously assigned to the Li_2S phase (JCPDS card # 23-0369). The background signal at low two-theta angles is due to Kapton tape used for protection from air. The *in situ* synthesis scheme combines pyrolysis and Li_2S formation in a one-step process. *In situ* processes have been employed for the synthesis of composites of carbon with various types of materials such as metal oxides and alloys.[20,21] This approach obviates separate creation of the carbon matrix and the active material and enhances the scalability of the synthesis process.

To determine the mass loading of Li_2S in the composite, TGA was performed for the composite and results are shown in ESI, Fig. S1.† In air, Li_2S is oxidized to Li_2SO_4 as confirmed by XRD and the weight fraction of Li_2S in the composite is calculated to be ~62%. Raman spectroscopy was used to investigate the nature of carbon obtained from pyrolysis of RF gel. Because Li_2S is hygroscopic and may affect the measurement, the Raman spectrum is taken (shown in Fig. 3) for the carbon pyrolyzed from RF gel synthesized using the same conditions (except that no Li_2SO_4 was added) at 900 °C for 2 h. The spectrum can be deconvoluted into peaks of Lorentzian shape centered at 1600, 1547 and 1350 cm^{-1}, which may be assigned to graphite (G), amorphous carbon (D3) and disordered graphitic lattice (D1), respectively.[22] The result indicates the partially graphitic nature of the carbon in the composite. The electrical conductivity of carbon obtained from pyrolyzing RF gel depends on factors such as pyrolysis temperature and density of product, and the value is generally on the order of 1–20 S cm^{-1} for a pyrolysis temperature of 800–900 °C.[23,24] In comparison, the electrical conductivity of carbon black is on the order of 1–5 S cm^{-1},[25] indicating that carbon derived from RF gel is a good candidate as a conductive supporting matrix for lithium sulfide. Besides electrical conductivity, the graphene layers present in the graphitic lattices can serve as substrates to which sulfur can be linked *via* carbon–sulfur interactions, which is helpful in the immobilization of sulfur/polysulfides.[10] The surface area and pore structure of the RF gel carbon composite were characterized using nitrogen adsorption and results are shown in ESI, Fig. S2.† The isotherm follows type-IV behavior with a type H4 hysteresis loop, which may indicate the presence of large

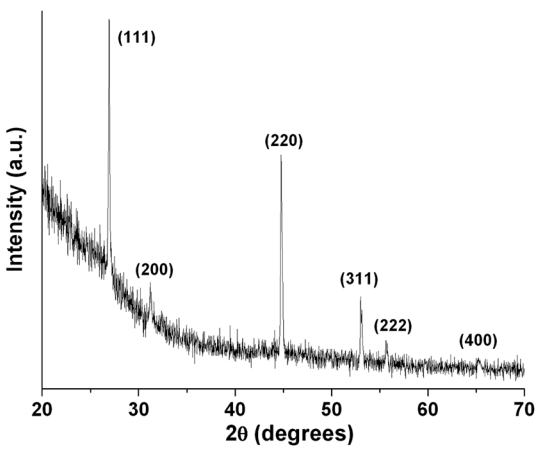

Fig. 2 X-Ray diffraction pattern of the Li_2S@C composite.

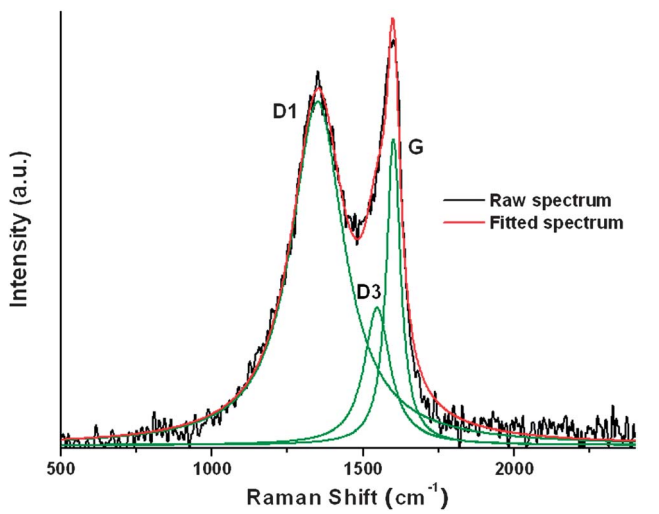

Fig. 3 Raman spectrum of carbon pyrolyzed from RF gel at 900 °C, deconvoluted into graphite (G), disordered graphitic lattice (D1) and amorphous carbon (D3) peaks.

mesopores embedded in a matrix of pores with much smaller size.[26] The pore size distribution shows that most of the pores are of size <6 nm. The BET surface areas of Li_2S@C composite and pure carbon are 336 and 830 $m^2\ g^{-1}$, respectively, indicating that the surface area of the composite is mainly attributed to that of the carbon, considering that the weight fraction of carbon in the composite is ~38%.

The morphology of the composite was studied using TEM and typical images are shown in Fig. 4(a) and (b). It is seen that the cross-linked RF gel generally forms spherical particles in the size range of 500 nm to 2 μm. To study the distribution of lithium sulfide in the carbon particles, Energy Dispersive X-Ray Spectroscopy (EDX) is performed on the particles and carbon and sulfur mappings are shown in Fig. 4(e) and (f), with the STEM image and EDX spectrum shown in Fig. 4(c) and (d). C and S maps show that sulfur is distributed throughout the carbon particles. Because of the relatively large size of the particles, it is difficult to distinguish in TEM the finer features of lithium sulfide within the bigger carbon particles. Lithium cannot be detected using EDX and Electron Energy Loss Spectroscopy (EELS) is used to investigate the presence of lithium. A line scan is performed on the composite for the presence of lithium (shown in ESI, Fig. S3(d)† based on the image in Fig. S3(a)† with EELS spectra shown in Fig. S3(b) and (c)†) and also indicates that lithium is distributed throughout the particles. An advantage which carbon could provide is that it could help to sequester the sulfur through formation of chemical bonding with sulfur and acting as a physical barrier for the diffusion of polysulfides.

The electrochemical performance of the as prepared Li_2S@C composite is shown in Fig. 5–7. Fig. 5 shows the cyclic voltammograms of Li_2S@C at different cycle numbers, which follow the commonly known reaction mechanism for lithiation of sulfur. At ~3 V the material exists as sulfur (S_8) and at ~1.5 V as Li_2S. The first anodic scan corresponds to the delithiation of Li_2S to form sulfur (peak at 2.75 V). In the cathodic scans, three peaks are distinguishable, at approximately 2.45 V, 2.1 V and 1.95 V, respectively. These peaks correspond to reduction of S_8 to higher order polysulfides (Li_2S_n, n = 5–8), higher order to lower order polysulfides (Li_2S_n, n = 2–4), and lower order polysulfides to Li_2S, respectively.[3,10,27–31] In the anodic scan, two peaks are distinguishable at approximately 2.4 V and 2.55 V and correspond to the oxidation of Li_2S to polysulfides and polysulfides to S_8. The cyclic voltammograms are consistent with the charge–discharge curves in Fig. 6(a), showing two reduction plateaus in discharge, at 2.45 V and 1.95 V, and two oxidation plateaus in discharge, at 2.3 V and 2.5 V. The decrease in peak area with cycle number in the CV scans corresponds to the decrease in discharge and charge capacities. Fig. 6(b) shows the charge–discharge curves for the physical mixture of Li_2S (62% by weight) and carbon pyrolyzed from RF gel at 900 °C (38% by weight).

Comparison of Fig. 6(a) and (b) clearly shows that the composites offer superior capacity and far superior ability to suppress the polysulfide shuttle. The cycling performance of the Li_2S@C composite and the physical mixture are compared in greater detail in Fig. 7(a). The charge–discharge rates are fixed at 0.5 C (1 C = 1166 mA g^{-1} Li_2S) and the capacity values reported are normalized with respect to the Li_2S active material mass. For the Li_2S@C composite, after 40 cycles the discharge capacity is 280 mA h g^{-1} compared to an initial discharge capacity of 330

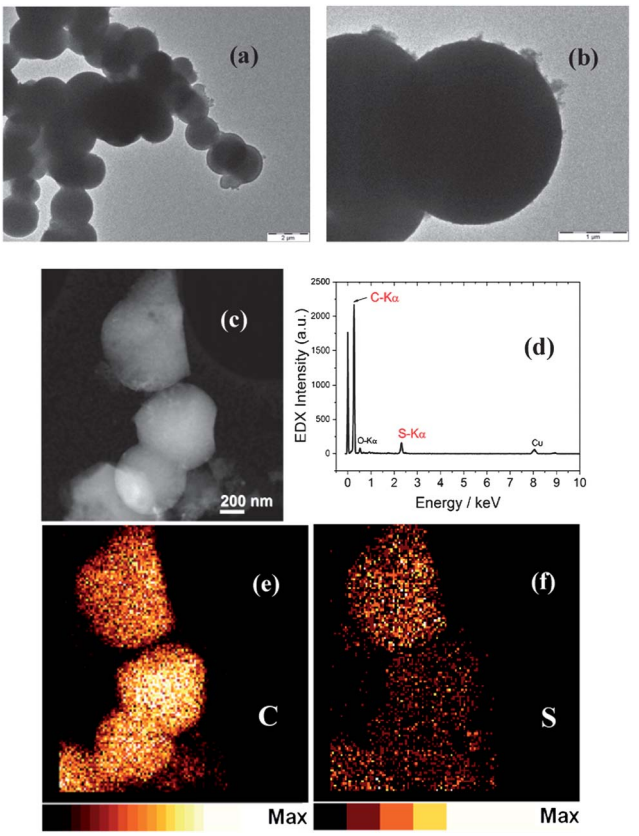

Fig. 4 (a and b) Transmission electron microscopy (TEM) images of Li_2S@C particles; (c) high angle annular dark field (HAADF) scanning transmission electron microscopy (STEM) image of Li_2S@C particles, along with (d) energy dispersive X-ray (EDX) spectrum, showing the presence of carbon K edge and sulfur K edge; EDX mapping of (e) carbon and (f) sulfur.

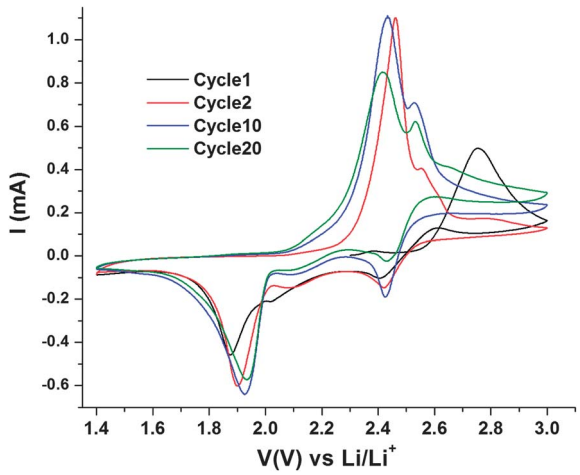

Fig. 5 Cyclic voltammograms of a Li_2S@C composite in 1 M LiTFSI in tetraglyme cycled at 0.2 mV s^{-1}.

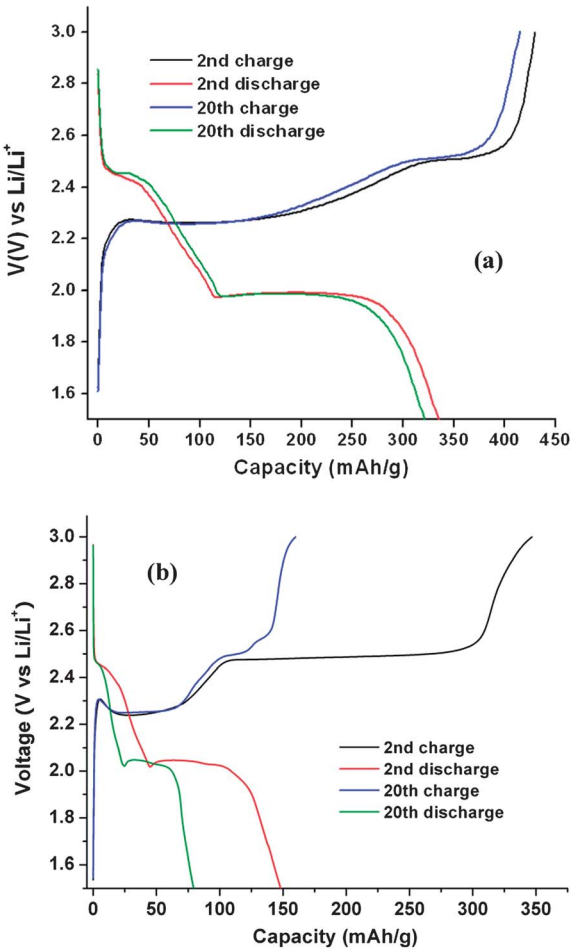

Fig. 6 Charge–discharge curves of (a) a Li_2S@C composite and (b) a physical mixture of Li_2S and carbon at 0.5 C charge–discharge rate. Electrolyte = 1 M LiTFSI in tetraglyme.

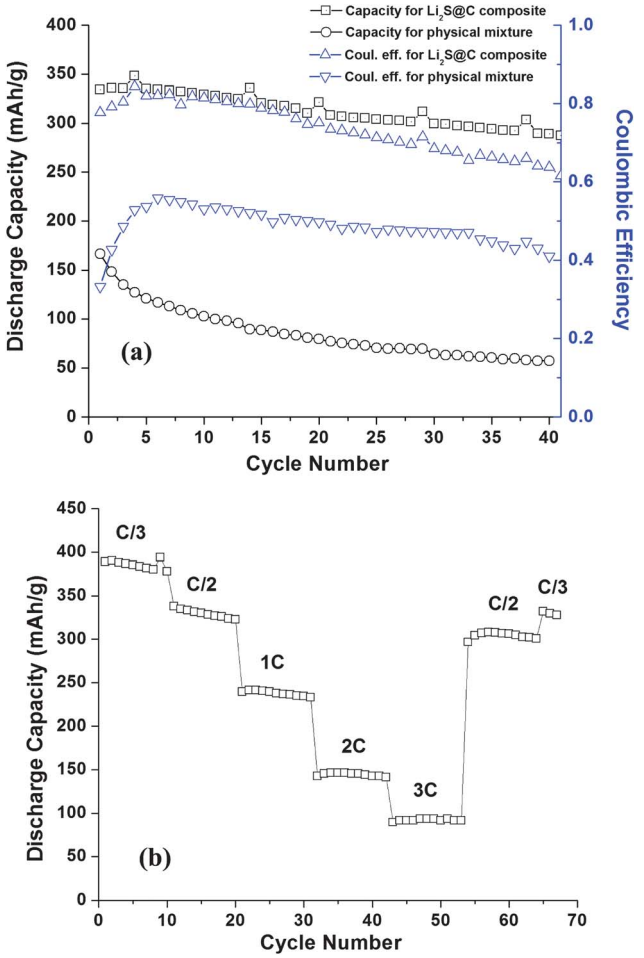

Fig. 7 (a) Cycling performance of a Li_2S@C composite and a physical mixture of Li_2S and carbon at 0.5 C (1 C = 1166 mA g^{-1}) charge–discharge rate; (b) cycling performance of a Li_2S@C composite at different charging rates. Electrolyte = 1 M LiTFSI in tetraglyme.

mA h g^{-1}. The coulombic efficiency decreases from 80% to 60% over the same number of cycles. The results show clear improvement over the physical mixture of Li_2S and carbon, but are far from optimum. Discharge capacities of the composite at different charging rates (C/3 to 3C) are shown in Fig. 7(b). Impedance plots for the composite and for physical mixtures of Li_2S with carbon (with the same electrode mass of 1.5 mg) before cycling and after 10 cycles are shown in ESI, Fig. S4.† Lower ohmic and charge transfer resistances are observed for the composite compared to the physical mixture, showing the effect of dispersing Li_2S in carbon on improving the conductivity of the material.

As in the lithium–sulfur cell, the composition of the electrolyte can have a profound effect on the solubility of lithium polysulfide Li_2S_n species, which in turn may have a large effect on the cell electrochemistry and stability. Additives such as $LiNO_3$ and ionic liquids have been proposed and shown to improve the cycling performance and coulombic efficiency of Li–S cells by limiting the loss of sulfur to the electrolyte.[3,32,33] Saturation levels of lithium polysulfides in the electrolyte should have as profound and perhaps a more predictable effect. Lithium polysulfides have been investigated as catholytes[34] as they are able both to serve as the electrolyte component and to deposit on the cathode in the reduced state as an active material. Lithium polysulfides dissolved in the electrolyte are also able to form a Li_2S–Li_2S_2 solid electrolyte interface film on a metallic lithium surface, as revealed by impedance studies, which can passivate and stabilize the surface.[35] Thus in addition to impeding loss of the active material from the cathode to the electrolyte, an electrolyte which already contains lithium polysulfides with the appropriate composition may also provide added benefits.

The synthesis protocol for lithium polysulfide used in this work is described in the Experimental section. Elemental analysis indicates that the overall composition of lithium polysulfides in the electrolyte is $Li_2S_{3.5}$, implying that Li_2S_n species with a distribution of n values above 2 are present in solution. UV-visible absorption spectra taken immediately after preparation of the electrolyte (with dilution to allow the absorbance to reach an appropriate range) are shown in Fig. 8. Deconvolution of the spectrum yields two peaks at ~615 nm and ~450 nm. The 615 nm peak is assigned to S_3^{2-}, while the peak at 450 nm corresponds to higher order polysulfides such

as S_5^{2-} or S_6^{2-}.[36,37] The ratio of the area under the curve for these two peaks is 4.1 : 1, which is consistent with the overall composition of the solution (n = 3.5 in Li_2S_n). The ionic conductivities of the Li_2S_n solutions in tetraglyme (with the same overall n ratio but different dilution ratios) were measured and are shown in ESI, Fig. S5† (all with 1 M LiTFSI). The ionic conductivities appear to follow a VFT-type relationship with temperature ($\sigma = A\exp(-B/(T - T_0))$). The fitting results are shown in the figure as lines with fitting parameters summarized in ESI, Table S1.† It is seen that the most concentrated lithium polysulfide solution (1.9 M $Li_2S_{3.5}$) has the lowest conductivity because of its high viscosity. As the polysulfide concentration becomes lower, the ionic conductivity of the solution approaches that of the bare LiTFSI–tetraglyme electrolyte.

The electrochemical performance of the Li_2S@C composite in 1 M LiTFSI + 0.095 M $Li_2S_{3.5}$ is shown in Fig. 9–11. The cyclic voltammograms (Fig. 9) show essentially the same peaks observed for the bare LiTFSI electrolyte, because polysulfides originally present in the electrolyte would also undergo similar reduction and oxidation reactions as polysulfides, which originate from the cathode. The polysulfides originally present in the electrolyte can be reduced to Li_2S/Li_2S_2 and deposited on the cathode and contribute to the apparent capacity measured (in addition to that contributed by the Li_2S originally present in the cathode). To account for this contribution, a control cathode was used, which contained only the RF gel carbon (no Li_2S), with the same mass as the carbon present in the Li_2S@C cathode. Specifically, on a 1.0 cm^2 aluminum electrode, 0.87 mg Li_2S@C is deposited, which contains 0.54 mg Li_2S and 0.33 mg carbon. The control cathode also contained 0.33 mg carbon, and 30 μL electrolyte is used for both cases, which contains 0.32 mg sulfur. The discharge capacities using the carbon cathode and Li_2S@C cathode are shown in Fig. 10, with a current density of 1.6 mA cm^{-2}, which is equivalent to 0.5C (1C = 1166 mA g^{-1} Li_2S) for the usual combination of Li_2S@C cathode with the 1 M LiTFSI electrolyte which has been used so far.

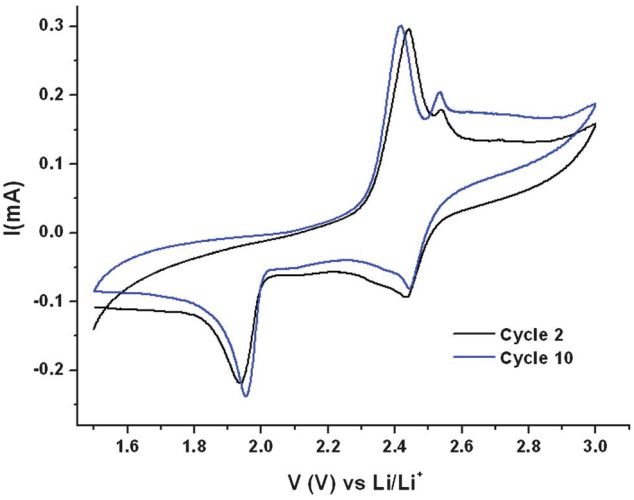

Fig. 9 Cyclic voltammograms of Li_2S@C in 1 M LiTFSI + 0.095 M $Li_2S_{3.5}$ in tetraglyme.

It is apparent from Fig. 10 that the carbon cathode with the polysulfide electrolyte shows exceptionally stable discharge capacities with no detectable decrease in 80 cycles, while the Li_2S@C cathode shows some fading. The discharge capacity due to the Li_2S in cathode is calculated by subtracting the capacity contribution of the carbon cathode from total capacity and is shown in Fig. 11, with the performance in bare LiTFSI electrolyte also shown for comparison. An electrolyte with 0.095 M of lithium polysulfide instead of higher polysulfide concentrations was used in order to ensure good ionic conductivity and to limit the capacity contributed by the electrolyte from overshadowing that of the Li_2S in the cathode. It is apparent from the figure that the electrolyte containing dissolved lithium polysulfide exhibits markedly lower capacity fading, compared to the electrolyte without $Li_2S_{3.5}$. The capacities of the carbon cathode and Li_2S@C cathode at different charging rates are shown in ESI,

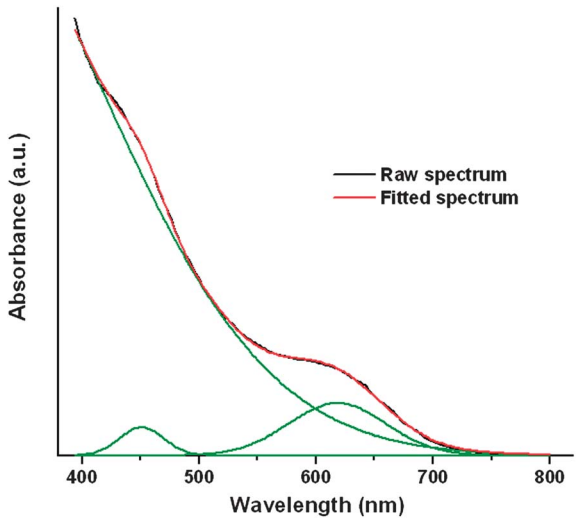

Fig. 8 UV-visible absorbance spectra of lithium polysulfide (9.5 mA $Li_2S_{3.5}$) in tetraglyme.

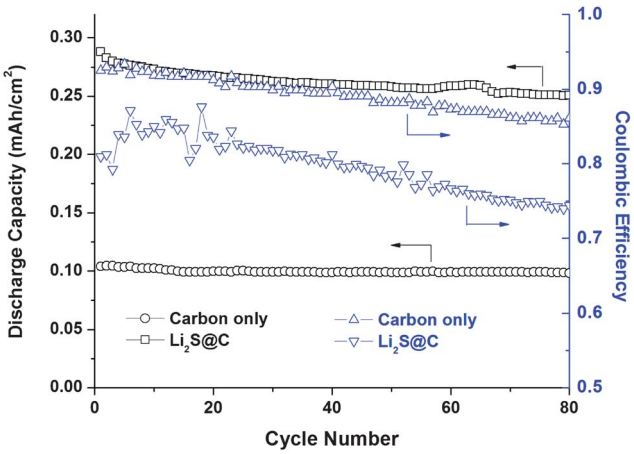

Fig. 10 Cyclic performance of carbon pyrolyzed from RF gel and Li_2S@C, respectively, in 1 M LiTFSI + 0.095 M $Li_2S_{3.5}$ in tetraglyme, at a charging rate of 0.16 mA cm^{-2}. Series in black corresponds to discharge capacity and series in blue corresponds to coulombic efficiency.

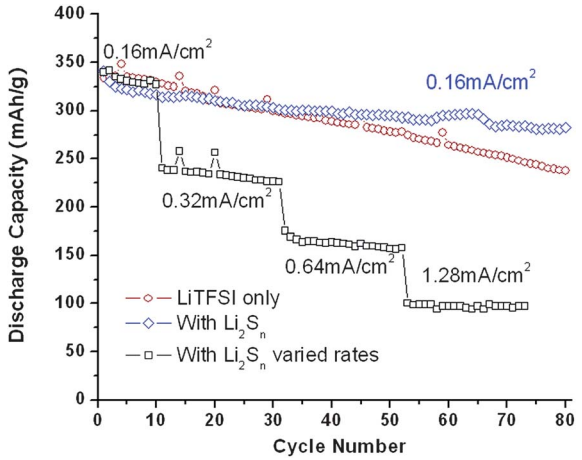

Fig. 11 Cycling performance of Li_2S@C with electrolytes without and with lithium polysulfides.

Fig. S6† and the difference in capacities for Li_2S@C and pure carbon, normalized by the electrode material mass, over the range of charge–discharge rates studied is shown in Fig. 11. The figure nicely shows that the presence of $Li_2S_{3.5}$ in the electrolyte stabilizes the cycling performance of Li_2S@C cathodes, without compromising the rate capability of the cathode.

Conclusion

We have developed a scalable, *in situ* method for creating lithium sulfide–carbon nanocomposites in which Li_2S is homogeneously dispersed in a mesoporous, partially graphitic carbon matrix. The matrix serves to enhance the electrical conductivity of the cathode and to sequester the active Li_2S material in the cathode. The effectiveness of the nanocomposite electrodes in inhibiting polysulfide shuttling and in improving the cycling stability of Li_2S is demonstrated through comparisons with the physical mixture of the material with carbon. We hypothesize that the success of our approach hinges on the homogeneous distribution of Li_2S in the carbon host. This distribution is thought to arise from specific interactions between the Li_2SO_4 precursor for Li_2S and the large concentration of polar oxygens in the resorcinol–formaldehyde aerogel used as a precursor for carbon. It is further shown that electrolyte compositions that incorporate lithium polysulfide as additives lead to additional improvements in cycling stability and efficiency of the Li_2S@C composite anodes.

Acknowledgements

This material is based on work supported as part of the Energy Materials Center at Cornell, an Energy Frontier Research Center funded by the U.S. Department of Energy, Office of Science, Office of Basic Energy Sciences under Award number DESC0001086. We also acknowledge the National Science Foundation, Partnerships for Innovation Program (Grant # IIP-1237622) for supporting the work on lithium polysulfide-based electrolyte additives for suppressing polysulfide shuttling.

References

1 M. Armand and J. M. Tarascon, *Nature*, 2008, **451**, 652.
2 Y. V. Mikhaylik and J. R. Akridge, *J. Electrochem. Soc.*, 2004, **151**, A1969.
3 D. Aurbach, E. Pollak, R. Elazari, G. Salitra, C. S. Kelley and J. Affinito, *J. Electrochem. Soc.*, 2009, **156**, A694.
4 J. H. Shin and E. J. Cairns, *J. Electrochem. Soc.*, 2008, **155**, A368.
5 J. L. Wang, J. Yang, J. Y. Xie and N. X. Xu, *Adv. Mater.*, 2002, **14**, 963.
6 L. F. Xiao, Y. L. Cao, J. Xiao, B. Schwenzer, M. H. Engelhard, L. V. Saraf, Z. M. Nie, G. J. Exarhos and J. Liu, *Adv. Mater.*, 2012, **24**, 1176.
7 X. L. Ji, K. T. Lee and L. F. Nazar, *Nat. Mater.*, 2009, **8**, 500.
8 N. Jayaprakash, J. Shen, S. S. Moganty, A. Corona and L. A. Archer, *Angew. Chem., Int. Ed.*, 2011, **50**, 5904.
9 R. Demir-Cakan, M. Morcrette, F. Nouar, C. Davoisne, T. Devic, D. Gonbeau, R. Dominko, C. Serre, G. Ferey and J. M. Tarascon, *J. Am. Chem. Soc.*, 2011, **133**, 16154.
10 L. W. Ji, M. M. Rao, H. M. Zheng, L. Zhang, Y. C. Li, W. H. Duan, J. H. Guo, E. J. Cairns and Y. G. Zhang, *J. Am. Chem. Soc.*, 2011, **133**, 18522.
11 J. C. Guo, Y. H. Xu and C. S. Wang, *Nano Lett.*, 2011, **11**, 4288.
12 L. W. Ji, M. M. Rao, S. Aloni, L. Wang, E. J. Cairns and Y. G. Zhang, *Energy Environ. Sci.*, 2011, **4**, 5053.
13 J. Schuster, G. He, B. Mandlmeier, T. Yim, K. T. Lee, T. Bein and L. F. Nazar, *Angew. Chem., Int. Ed.*, 2012, **51**, 3591.
14 J. Hassoun, Y. K. Sun and B. Scrosati, *J. Power Sources*, 2011, **196**, 343.
15 Y. Yang, M. T. McDowell, A. Jackson, J. J. Cha, S. S. Hong and Y. Cui, *Nano Lett.*, 2010, **10**, 1486.
16 Y. Yang, G. Y. Zheng, S. Misra, J. Nelson, M. F. Toney and Y. Cui, *J. Am. Chem. Soc.*, 2012, **134**, 15387.
17 T. Takeuchi, H. Sakaebe, H. Kageyama, H. Senoh, T. Sakai and K. Tatsumi, *J. Power Sources*, 2010, **195**, 2928.
18 S. A. Al-Muhtaseb and J. A. Ritter, *Adv. Mater.*, 2003, **15**, 101.
19 A. M. ElKhatat and S. A. Al-Muhtaseb, *Adv. Mater.*, 2011, **23**, 2887.
20 Z. C. Yang, J. G. Shen, N. Jayaprakash and L. A. Archer, *Energy Environ. Sci.*, 2012, **5**, 7025.
21 S. K. Das, R. Mallavajula, N. Jayaprakash and L. A. Archer, *J. Mater. Chem.*, 2012, **22**, 12988.
22 A. Sadezky, H. Muckenhuber, H. Grothe, R. Niessner and U. Poschl, *Carbon*, 2005, **43**, 1731.
23 S. J. Kim, S. W. Hwang and S. H. Hyun, *J. Mater. Sci.*, 2005, **40**, 725.
24 H. Probstle, M. Wiener and J. Fricke, *J. Porous Mater.*, 2003, **10**, 213.
25 J. Sanchez-Gonzalez, A. Macias-Garcia, M. F. Alexandre-Franco and V. Gomez-Serrano, *Carbon*, 2005, **43**, 741.
26 M. Kruk and M. Jaroniec, *Chem. Mater.*, 2001, **13**, 3169.
27 C. Lai, X. P. Gao, B. Zhang, T. Y. Yan and Z. Zhou, *J. Phys. Chem. C*, 2009, **113**, 4712.
28 Y. J. Choi, Y. D. Chung, C. Y. Baek, K. W. Kim, H. J. Ahn and J. H. Ahn, *J. Power Sources*, 2008, **184**, 548.

29 Y. J. Jung and S. Kim, *Electrochem. Commun.*, 2007, **9**, 249.
30 H. Yamin and E. Peled, *J. Power Sources*, 1983, **9**, 281.
31 X. M. He, W. H. Pu, J. G. Ren, L. Wang, J. L. Wang, C. Y. Jiang and C. R. Wan, *Electrochim. Acta*, 2007, **52**, 7372.
32 Y. V. Mikhaylik, *US Pat.* no. 7,354,680, 2008.
33 J. H. Shin and E. J. Cairns, *J. Power Sources*, 2008, **177**, 537.
34 R. D. Rauh, K. M. Abraham, G. F. Pearson, J. K. Surprenant and S. B. Brummer, *J. Electrochem. Soc.*, 1979, **126**, 523.
35 V. S. Kolosnitsyn, E. V. Kuzmina, E. V. Karaseva and S. E. Mochalov, *J. Power Sources*, 2011, **196**, 1478.
36 R. D. Rauh, F. S. Shuker, J. M. Marston and S. B. Brummer, *J. Inorg. Nucl. Chem.*, 1977, **39**, 1761.
37 C. Barchasz, F. Molton, C. Duboc, J. C. Lepretre, S. Patoux and F. Alloin, *Anal. Chem.*, 2012, **84**, 3973.